A Ceramic-Based Separator for High-Temperature Supercapacitors

Bin Qin[+],[a, b] Yu Han[+],[a, b] Yuxin Ren[+],[a, b] Dong Sui,[a, b] Ying Zhou,[a, b] Miao Zhang,[a, b] Zhenhe Sun,[a, b] Yanfeng Ma,[a, b] and Yongsheng Chen*[a, b]

Currently, supercapacitors have the shortcoming of limited operation temperature mainly owing to the low thermal stability of separators, which seriously hinder their application at high temperatures. In this work, a simple and universal method for the fabrication of high-temperature standing ceramic-based separators is reported. It was demonstrated that such a separator can withstand over 350 °C without any shrinkage. Supercapacitors fabricated by using such separators can be operated at as high as 120 °C efficiently and even after 9000 cycles at 2.5 V operation voltage, their capacitance still retained approximately 88 % of their initial performance. To the best of our knowledge, this is the first report of a separator with such high thermal stability.

Introduction

Supercapacitors (SCs) have drawn extensive attention owing to their high power density and long cycle life.[1–6] What is more, high-temperature supercapacitors (HTSCs) that could satisfy some special requirements in drilling, space, and military applications are also very desirable. Unfortunately, reports of HTSCs with temperature tolerance above 120 °C are limited up to now.[7–11] To make HTSCs work efficiently, the electrolyte, packing case, active materials, and separator all have to be thermally and electrochemically stable. Electrolytes of HTSCs mainly include polymer-based solid electrolytes[8,10,11] and ionic liquids;[9,12,13] for comparison, conventional electrolytes are generally acetonitrile and polypropylene carbonate (PC).[14,15] Packing case materials of HTSCs primarily consist of aluminum,[16] stainless steel,[14] and polymer films,[10,11] all of which possess excellent thermally stability. As for the active materials of HTSCs, commercial activated carbon,[7] activated carbon fabrics,[14] carbon nanotubes,[17] carbon nano-onions,[18] and reduced graphene oxide[11] all have been studied. Most importantly, separators, which need to possesses high thermal stability, low resistance to ion transportation, perfect wettability, strong tensile strength, and good flexibility,[19] have severely been hindering the development of HTSCs.

There are several types of separators that may be considered for HTSCs, but they all have some shortcomings. Commercial separators such as polyolefin-based porous films and cellulose paper are not good choices for high-temperature applications because they can easily shrink at high temperatures and consequently lead to electrical short circuits inside the devices.[9,20] Although ceramic coatings on polyolefin-based porous films can improve the thermal stability of the separator to some extent,[20] they still cannot meet the special requirement of HTSCs in terms of thermal stability. Glass fiber membranes[14,21,22] have been commonly used as separators for HTSCs because of their outstanding thermal and electrochemical stability, and HTSCs fabricated by using glass fiber films exhibit excellent cycling stability. However, the main weakness of the glass fiber membrane was its poor flexibility and relatively low tensile strength, which impede the fabrication of rolled devices. Porous alumina[18,23] possesses outstanding thermal stability and has also been studied as a separator of HTSCs, but it is extremely brittle and expensive. Porous polytetrafluoroethylene (PTFE) films seem to be a promising candidate for HTSC separators, but HTSCs using a PTFE film as separator have been rarely reported to date,[24] probably owing to the low wettability between the PTFE film and electrolyte. Phosphoric acid-doped polymer,[8,10,11] clay-doped polymer,[9] and SiO_2-doped polymer composites[12,25] all have been studied as high-temperature separators but they have the shortcomings of low operation voltage, large thickness, high resistance, and lack of flexibility.

To address the issues confronting separators of HTSCs, we report herein a simple and universal method for the fabrication of ceramic nanoparticles (NPs)/PTFE separator that is composed of spider-web-like PTFE binder with ceramic NPs

[a] B. Qin,[+] Y. Han,[+] Y. X. Ren,[+] Dr. D. Sui, Dr. Y. Zhou, Dr. M. Zhang, Z. H. Sun, Prof. Dr. Y. F. Ma, Prof. Dr. Y. S. Chen
The Centre of Nanoscale Science and Technology and Key Laboratory of Functional Polymer Materials
State Key Laboratory and Institute of Elemento-Organic Chemistry
College of Chemistry, Nankai University
Tianjin, 300071 (P.R. China)
E-mail: yschen99@nankai.edu.cn

[b] B. Qin,[+] Y. Han,[+] Y. X. Ren,[+] Dr. D. Sui, Dr. Y. Zhou, Dr. M. Zhang, Z. H. Sun, Prof. Dr. Y. F. Ma, Prof. Dr. Y. S. Chen
The National Institute for Advanced Materials, Nankai University
Tianjin 300071 (P.R. China)

[+] These authors contributed equally to this work.

Supporting information for this article can be found under: https://doi.org/10.1002/ente.201700438.

entangled inside. Two types of ceramic NPs were studied, including fumed silicon dioxide (SiO_2) and silicon carbide (SiC) NPs. As-prepared separators can withstand over 350 °C without any shrinkage. Furthermore, the separator shows exceptional flexibility, high tensile strength, high wettability to electrolyte, and low resistance to ion transportation during charging/discharging, all of which can be attributed to the unique structure of the ceramic NPs/PTFE separator. Supercapacitors fabricated by using such a separator can be operated at 120 °C efficiently and even after 9000 cycles at 120 °C and 2.5 V, the capacitance still retained approximately 88 % of its initial value.

Results and Discussion

Fabrication and microstructure of ceramic NPs/PTFE

The fabrication process of the ceramic NPs/PTFE separator is illustrated in Scheme 1. It mainly involves three steps: firstly, ceramic NPs and PTFE powder were homogeneously mixed and ground in the presence of a small amount of ethanol in agate mortar; secondly, the mixture was rolled and folded repeatedly to obtain the ceramic NPs/PTFE film; lastly, the as-prepared film was further pressed under 15 MPa to obtain the ceramic NPs/PTFE separator. In this work, two types of ceramic NPs were studied including fumed SiO_2 and SiC NPs and there is no significant difference in microstructure between these two mentioned separators.

Figure 1 shows the typical SEM images of fumed SiO_2/PTFE (80:20 wt %) separator. The top-view images (Figure 1 a, b) indicate that this separator was composed of SiO_2 NPs with the diameter of approximately 25 nm (particle size distribution in Figure S1, Supporting Information) and there are many nanoscale spaces between these NPs. These spaces between the SiO_2 particles can provide sufficient ion transportation paths during the charging/discharging process. Moreover, SiO_2 NPs also increases the degree of wetting between separator and electrolyte owing to the surface silanol groups.[26,27] Sufficient ion paths and perfect wettability of the separator ensure the low internal resistance of SCs. On the other hand, cross-sectional images (Figure 1 c, d) show that these SiO_2 NPs were actually entangled inside spider-web-like PTFE binder. The unique structure of the spider-web-like PTFE entangling SiO_2 NPs not only provides sufficient mechanical strength from the PTFE, but also retains the nanoscale spaces between the SiO_2 NPs without the blocking of ion path by aggregated polymer binder. The SiC NPs/PTFE separator (Figure S2, Supporting Information) possesses the same microstructure as the fumed SiO_2/PTFE separator.

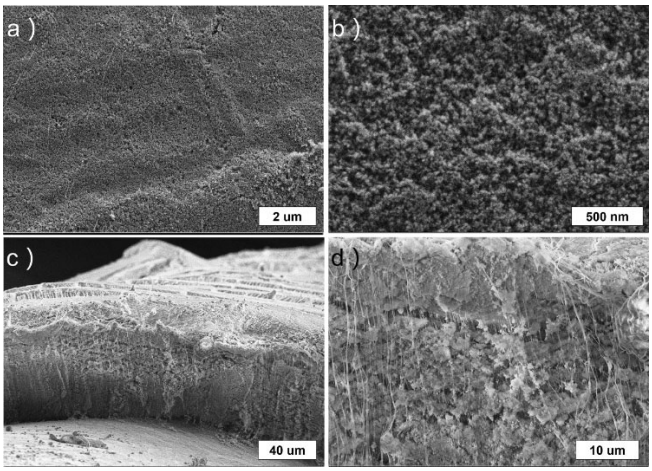

Figure 1. Typical SEM images of fumed SiO_2/PTFE (80:20 wt %) separator from (a, b) top view, and (c, d) cross-sectional view.

Physical properties of ceramic NPs/PTFE

The physical properties of the ceramic NPs/PTFE separators were systematically investigated, including the thermal stability, tensile strength, wettability, permeability, and porosity. Figure 2 a shows the thermogravimetric (TG) and differential thermal analysis (DTA) curves of the fumed SiO_2/PTFE (80:20 wt %) separator in an air atmosphere at a heating rate of 10 K min^{-1}. The TG curve indicates that there is only 3 % weight losses between room temperature (RT) and 400 °C where the decomposition of PTFE starts.[28] These losses within 400 °C are attributed to the release of physically adsorbed water and the dehydroxylation of surface OH groups in SiO_2 NPs.[27] At approximately 522 °C, the decomposition of PTFE reaches its peak and the lost weight of PTFE in the separator is 23 %, close to the initially designed ratio of fumed SiO_2 and PTFE (80:20 wt %). The DTA curve indicates the melting point (T_m) of PTFE at 325 °C and again the decomposition peak at 522 °C.[28] Both TG and DTA imply that this separator possesses excellent thermal stability and can possibly be used at temperatures higher than 325 °C.

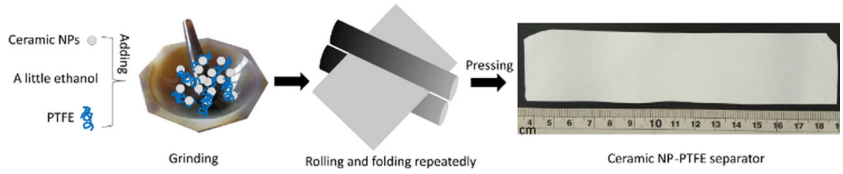

Scheme 1. Schematic illustration of the fabrication process for ceramic NPs/PTFE separators. It mainly involves three steps: firstly, ceramic NPs and PTFE powder were homogeneously mixed and ground together in the presence of a small amount of ethanol in an agate mortar; secondly, the mixture was rolled and folded repeatedly to obtain the ceramic NPs/PTFE film; lastly, the as-prepared film was further pressed under 15 MPa to obtain the ceramic NPs/PTFE separator.

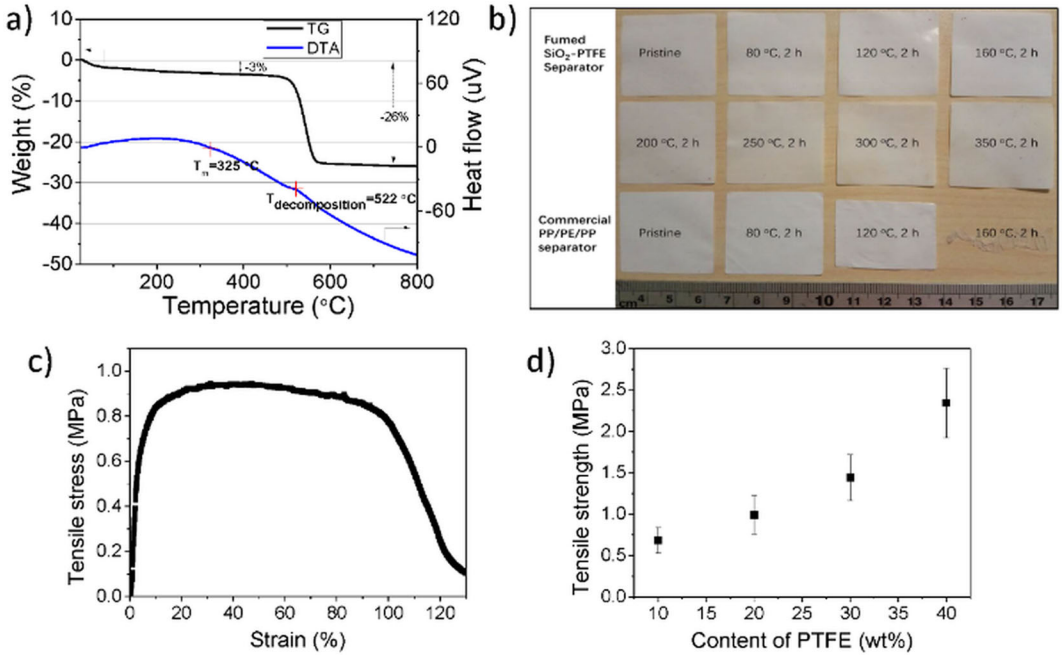

Figure 2. (a) TG and DTA curves of the fumed SiO_2/PTFE (80:20 wt%) separator at a heating rate of 10 K min^{-1} in air. (b) Digital photographs of the fumed SiO_2/PTFE (80:20 wt%) separator and commercial PP/PE/PP separator, treated under various temperatures. (c) Typical tensile stress–strain curve for the fumed SiO_2/PTFE (80:20 wt%) separator. d) Tensile strength of the fumed SiO_2/PTFE separator versus the content of PTFE in the separator.

Changing the testing atmosphere to N_2 did not show significant variation in the TG and DTA results (Figure S3, Supporting Information). Figure 2b shows the thermal shrinkage photographs of the fumed SiO_2/PTFE (80:20 wt%) separator. Clearly, it shows no shrinkage even after exposure to 350 °C for 2 h. In comparison, a commercial polypropylene (PP)/polyethylene (PE)/PP separator shows significant shrinkage (21%) at 120 °C and was observed to be completely destroyed at 160 °C.

Figure 2c shows a typical tensile stress–strain curve for fumed SiO_2/PTFE (80:20 wt%) separator. The tensile strength is approximately 1.0 MPa for 20 wt% content of PTFE and no significant difference was observed between the machine direction (MD) and the transverse direction (TD). Figure 2d is the relationship between tensile strength and the content of PTFE in the separator. The tensile strength becomes larger with more PTFE added to the separator and 20 wt% content here was determined as the optimal ratio of fumed SiO_2 and PTFE, because more PTFE would dramatically decrease the wettability between the electrolyte and separator (Figure S4, Supporting Information) and less PTFE would not only reduce the tensile strength but also increase the difficulty of preparing such a separator, as encountered in our experiments. In addition to the good tensile strength, the fumed SiO_2/PTFE separator also possesses outstanding flexibility (Figure S5, Supporting Information), which is especially important for HTSC applications because the fabrication of energy storage devices usually involves the winding of the separator,[29] which requires good flexibility. The SiC NPs/PTFE separator shows similar physical properties in terms of thermal stability (Figure S6a,b and Figure S7), tensile strength (Figure S6c,d), and wettability (Figure S4), all shown in the Supporting Information.

Table 1 compares the essential physical properties of the ceramic NPs/PTFE (80:20 wt%) separators and commercial PP/PE/PP separator. The air permeability of the fumed SiO_2/PTFE separator, one of the essential factors for evaluating the pore structure in separators,[30,31] was determined to have a Gurley value of 436 s per 100 mL, which was somewhat

Table 1. Physical properties of the fumed SiO_2/PTFE (80:20 wt%) separator, SiC NPs/PTFE (80:20 wt%) separator, and commercial PP/PE/PP separator.

	Thickness [μm]	Gurley value [s (100 mL)$^{-1}$]	Porosity [%]	Tensile strength [MPa]		Thermal shrinkage[a] [%]		Electric strength [kV mm^{-1}]
				MD	TD	MD	TD	
fumed SiO_2/PTFE separator	85 ± 10	436 ± 175	63 ± 2	1.0 ± 0.2	1.0 ± 0.2	0	0	11.0 ± 0.7
SiC NPs/PTFE separator	85 ± 10	430 ± 112	50 ± 1	1.3 ± 0.5	1.3 ± 0.5	0	0	20.3 ± 5.8
commercial PP/PE/PP separator[b]	25	620	39	167	15	21 (120 °C, 2 h)	0 (120 °C, 2 h)	105.0 ± 6.8

[a] At 350 °C for 2 h unless stated otherwise. [b] The data was obtained using Celgard 2325 except thermal shrinkage and electric strength, both of which were measured in our experiments.

less than the commercial PP/PE/PP separator (620 s per 100 mL). A lower Gurley value implies potentially more ion transport paths in the as-fabricated separator.[30,31] The porosity of the as-fabricated separator was measured by using n-butanol uptake. In this regard, the fumed SiO_2/PTFE separator allowed 63 % uptake, which is larger than the commercial PP/PE/PP separator (39 %), thereby implying higher capacity for holding the electrolyte and faster ionic transportation.[30] The SiC NPs/PTFE separator displays similar properties to the fumed SiO_2/PTFE separator as shown in Table 1. In conclusion, the ceramic NPs/PTFE (80:20 wt %) separators show excellent thermal stability (zero shrinkage at 350 °C for 2 h), good tensile strength (1.0 and 1.3 MPa for SiO_2- and SiC-based separators, respectively), relatively high air permeability (436 and 430 s per 100 mL for SiO_2- and SiC-based separators, respectively), and high porosity (63 % and 50 % for SiO_2- and SiC-based separators, respectively), all of which are crucial for application in HTSCs.

Cyclic voltammetry and impedance spectroscopy

Figure 3 a shows the CV curves of HTSCs (structure in Figure S8, Supporting Information) when using the fumed SiO_2/PTFE separator at a scan rate of 50 mV s^{-1} under different temperatures. The CV curves at the scan rate of 50 mV s^{-1} are rectangular for all temperatures from room temperature to 150 °C, implying ideal capacitive properties.[32] Moreover, there are no noticeable upward currents even at 150 °C when the voltage approaches 2.5 V; this means that there is no side reaction during the charge/discharge process at high temperatures. Other scan rates such as 25 mV s^{-1} and 100 mV s^{-1} are presented in Figure S9 (Supporting Information). Figure 3 b shows the Nyquist plots of HTSCs for the fumed SiO_2/PTFE separator. Both the solution resistance of the electrolyte (R_s) presented by the real axis intercept at high frequencies,[14,33] and the charge transfer resistance (R_{ct}) displayed by the semi-circle loop span along real axis[14,17] continuously decrease as the temperature increases. Such decreases of R_s and R_{ct} indicate that the internal resistance of the HTSCs will reduce with increases in temperature. Therefore, at high temperatures SCs should exhibit better performance than at room temperature. The vertical part of the curve at low frequencies represents the capacitive properties of supercapacitors;[34] and indicates that the HTSCs using the fumed SiO_2/PTFE separator possess ideal capacitive properties from room temperature to 150 °C as the electrochemical impedance spectroscopy (EIS) curves at low frequencies are nearly vertical for all temperatures. CV and EIS measurements of HTSCs using the SiC NPs/PTFE separator show similar results to the fumed SiO_2/PTFE separator (Figure S10, Supporting Information).

Constant-current charge/discharge testing

Figure 4 a,b shows the constant-current charge/discharge (CC) tests of HTSCs using the fumed SiO_2/PTFE separator with voltages of 2.5 V at different temperatures. The discharge specific capacitance firstly increases as the temperature elevates and then gradually approaches a constant value. For example, the discharge capacitance is approximately 70 F g^{-1} at room temperature and it increases to approximately 100 F g^{-1} when the temperature reaches 120 °C. A further increase of the temperature does not remarkably improve the discharge specific capacitance but decreases the Coulombic efficiency instead (Figure 4 a). CC curves all present constant slopes from room temperature to 150 °C (Figure 4 b), also indicating ideal capacitive properties for all researched operation temperatures.[35] Considering the above CC results at different temperatures, the cycle stability of HTSCs using the fumed SiO_2/PTFE separator was tested at a temperature of 120 °C and voltage of 2.5 V. Figure 4 c shows that the initial discharge specific capacitance is 78 F g^{-1} and even after 9000 cycles at 2.5 V operation voltage, its capacitance still retained approximately 88 % of the initial value. Moreover, the CC curves (Figure 4 d) display favorable triangle shapes for all cycles, indicating that there is no dramatic change of the capacitive properties in the HTSCs. Replacing the fumed SiO_2/PTFE separator with the SiC NPs/PTFE separator also yields outstanding high-temperature cycling stability as shown in Figure S11 (Supporting Information). In

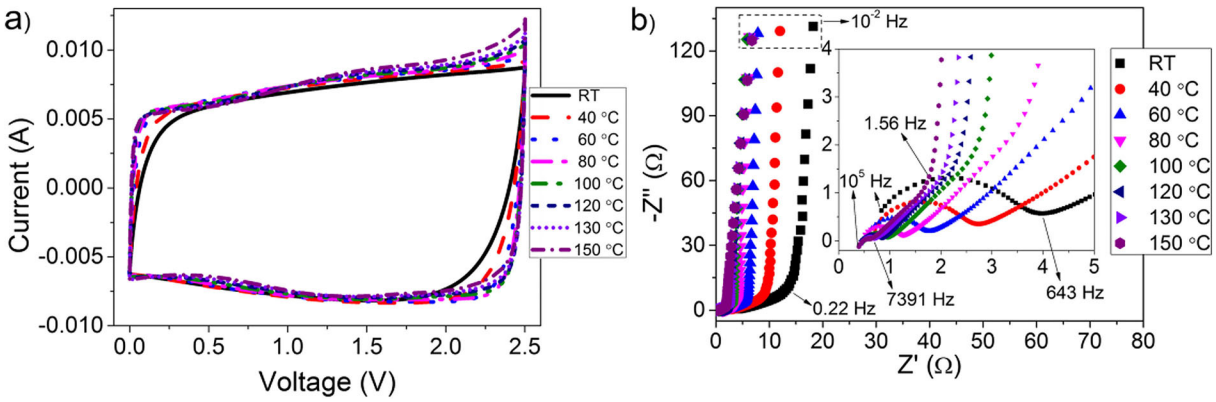

Figure 3. (a) CV curves of HTSCs using the fumed SiO_2/PTFE (80:20 wt %) separator at a scan rate of 50 mV s^{-1} under different temperatures. (b) Nyquist plots obtained after CV tests at different temperatures.

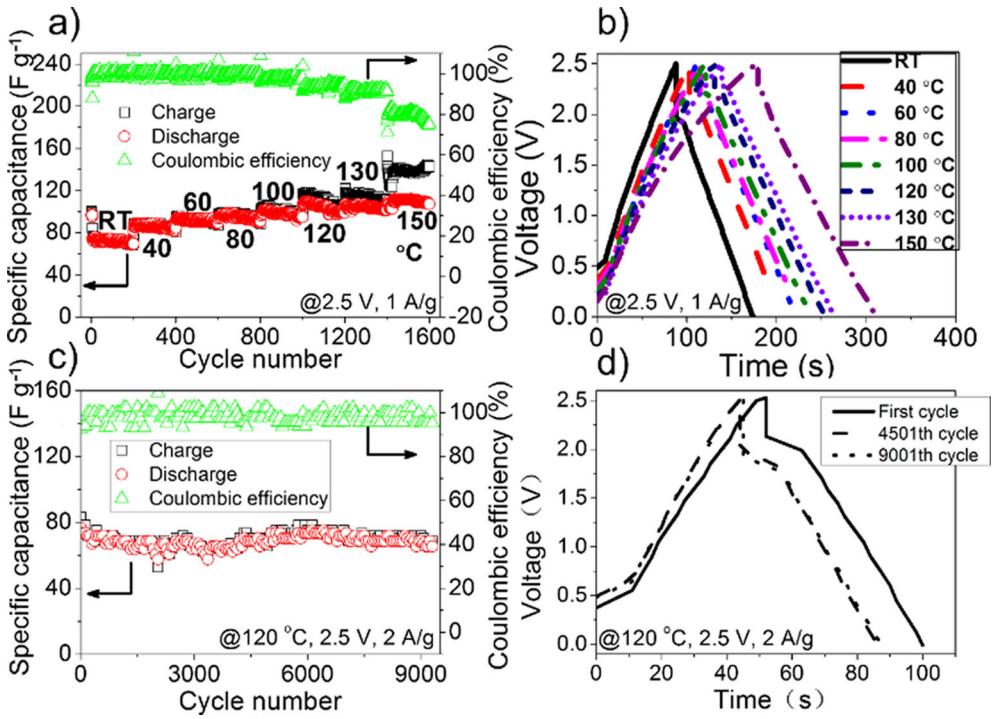

Figure 4. (a, b) CC tests of HTSCs using the fumed SiO_2/PTFE (80:20 wt%) separator at different temperatures. (c, d) Cycle stability of HTSCs using the fumed SiO_2/PTFE (80:20 wt%) separator at 120 °C.

summary, separators fabricated by using fumed SiO_2/PTFE and SiC/PTFE both exhibited excellent cycle stability at 120 °C, implying that the method developed here has the potential to be applied to other ceramic NPs in addition to fumed SiO_2 and SiC.

Conclusions

A simple and universal method for fabricating ceramic NPs/PTFE separators was reported. The as-prepared separator was composed of spider-web-like PTFE binder with ceramic NPs entangled inside. Excellent thermal, physical, and electrochemical properties were obtained for such separators, which make them nearly ideal candidates for high-temperature supercapacitor (HTSC) applications. Supercapacitors fabricated by using ceramic NPs/PTFE separators, including the fumed SiO_2/PTFE separator and SiC NPs/PTFE separator, can be operated at 120 °C efficiently with exceptional capacitance retention. We believe the method developed here is applicable to other ceramic NPs in addition to fumed SiO_2 and SiC NPs and this may also yield a new way for designing better HTSC separators.

Experimental Section

Preparation of ceramic NPs/PTFE separators

Fumed SiO_2 (Aladdin, hydrophilic) or SiC NPs (Macklin) and PTFE (Dupont) with certain ratios (ceramic NPs/PTFE = 9:1, 8:2, 7:3, and 6:4 wt%) were homogeneously mixed in an agate mortar with the presence of a small quantity of ethanol. Then, the mixture was rolled and folded repeatedly to obtain the separator. After that, the separator was further pressed with 15 MPa pressure until a smooth surface was achieved, which was cut to the desired size. The separator was dried at 120 °C for more than 3 h before being used in the HTSCs. The pure PTFE separator was prepared by the same method as the ceramic NPs/PTFE separators but without the addition of ceramic the NPs.

Fabrication of HTSCs

Briefly, 85 wt% activated carbon YP50 (Kuraray Chemicals), 10 wt% PTFE (Dupont), and 5 wt% carbon black (Super P, Timcal) were homogeneously mixed in an agate mortar and the mixture was rolled into a sheet of 60–80 mm thickness, which was punched into 12 mm diameter electrodes. The electrodes were hot pressed onto an aluminum current collector that contains conducting carbon coated on the surface and dried at 180 °C for 6 h under vacuum. The HTSCs consisted of two identical electrodes and a separator, all of which were sandwiched between two aluminum plates (schematic structure in Figure S8, Supporting Information). 1-Ethyl-3-methylimidazolium bis(trifluoromethylsulfonyl)imide (EMIMTFSI, Lanzhou Greenchem ILs) was used as the electrolyte. The HTSCs were fabricated in a glovebox filled with Ar.

Measurement of HTSCs

CC tests were performed using a LAND battery testing system. CV and EIS tests were conducted by using an Autolab (Metrohm). EIS was measured from 100 kHz to 10 mHz with an alternating voltage of 10 mV. For the CC tests, the gravimetric specific capacitance, C_s ($F g^{-1}$), was calculated according to Equation (1):

$$C_S = \frac{4I}{m\,dV/dt} \quad (1)$$

in which I is the constant current (A), m is the total mass of two electrodes (g), dV/dt (Vs^{-1}) is the slope obtained by fitting a straight line to the charge or discharge curve.

Characterization

The surface and cross-sectional morphologies of the separators were characterized by SEM (Zeiss Supra55 or PhenomPro). Thermal stability was measured by using TG and DTA (Rigaku TG8121). Tensile strength was obtained from the stress–strain curves tested by using a single-fiber tension machine (LLY-06ED, Lai zhou electron instrument). The air permeability was examined using a Gurley densometer (Gurley-4110N). Porosity was determined by using n-butanol uptake. Electric strength was measured by applying a gradually increased voltage with direct current until the breakdown of the separator.

Acknowledgements

The authors gratefully acknowledge financial support from the Ministry of Science and Technology of China (MoST, 2016YFA0200200), the National Natural Science Foundation of China (NSFC, 51633002, 51472124, 5127309, and 21374050), 111 Project (#B12015), and Tianjin 16ZXCLGX00100.

Conflict of interest

The authors declare no conflict of interest.

Keywords: electrochemistry · energy storage · ceramic separators · supercapacitors · thermal stability

[1] Y. Liu, Z. Wang, Y. Zhong, M. Tade, W. Zhou, Z. Shao, Adv. Funct. Mater. **2017**, 27, 1701229.
[2] L. Zhang, F. Zhang, X. Yang, G. Long, Y. Wu, T. Zhang, K. Leng, Y. Huang, Y. Ma, A. Yu, Y. Chen, Sci. Rep. **2013**, 3, 1408.
[3] Y. Wang, Z. Shi, Y. Huang, Y. Ma, C. Wang, M. Chen, Y. Chen, J. Phys. Chem. C **2009**, 113, 13103.
[4] Z.-S. Wu, W. Ren, L. Gao, J. Zhao, Z. Chen, B. Liu, D. Tang, B. Yu, C. Jiang, H.-M. Cheng, ACS Nano **2009**, 3, 411.
[5] Y. Lu, F. Zhang, T. Zhang, K. Leng, L. Zhang, X. Yang, Y. Ma, Y. Huang, M. Zhang, Y. Chen, Carbon **2013**, 63, 508.
[6] Y. Liu, J. Dinh, M. O. Tade, Z. Shao, ACS Appl. Mater. Interfaces **2016**, 8, 23774.
[7] X. Liu, Z. Wen, D. Wu, H. Wang, J. Yang, Q. Wang, J. Mater. Chem. A **2014**, 2, 11569.
[8] R. S. Hastak, P. Sivaraman, D. D. Potphode, K. Shashidhara, A. B. Samui, Electrochim. Acta **2012**, 59, 296.
[9] R. S. Borges, A. L. Reddy, M. T. Rodrigues, H. Gullapalli, K. Balakrishnan, G. G. Silva, P. M. Ajayan, Sci. Rep. **2013**, 3, 2572.
[10] T. Hibino, K. Kobayashi, M. Nagao, S. Kawasaki, Sci. Rep. **2015**, 5, 7903.
[11] S.-K. Kim, H. J. Kim, J.-C. Lee, P. V. Braun, H. S. Park, ACS Nano **2015**, 9, 8569.
[12] B. Shen, R. Guo, J. Lang, L. Liu, L. Liu, X. Yan, J. Mater. Chem. A **2016**, 4, 8316.
[13] M. Armand, F. Endres, D. R. MacFarlane, H. Ohno, B. Scrosati, Nat. Mater. **2009**, 8, 621.
[14] K. Hung, C. Masarapu, T. Ko, B. Wei, J. Power Sources **2009**, 193, 944.
[15] R. Kötz, M. Hahn, R. Gallay, J. Power Sources **2006**, 154, 550.
[16] B. Qin, X. Wang, D. Sui, T. Zhang, M. Zhang, Z. Sun, Z. Ge, Y. Xie, Y. Zhou, Y. Ren, Y. Han, Y. Ma, Y. Chen, Energy Technol. **2017**, https://doi.org/10.1002/ente.201700368.
[17] C. Masarapu, F. Z. Hai, H. H. Kai, B. Wei, ACS Nano **2009**, 3, 2199.
[18] R. Lin, P. L. Taberna, S. Fantini, V. Presser, C. R. Pérez, F. Malbosc, N. L. Rupesinghe, K. B. K. Teo, Y. Gogotsi, P. Simon, J. Phys. Chem. Lett. **2011**, 2, 2396.
[19] P. Arora, Z. Zhang, Chem. Rev. **2004**, 104, 4419.
[20] C. Yang, H. Tong, C. Luo, S. Yuan, G. Chen, Y. Yang, J. Power Sources **2017**, 348, 80.
[21] A. Balducci, R. Dugas, P. L. Taberna, P. Simon, D. Plée, M. Mastragostino, S. Passerini, J. Power Sources **2007**, 165, 922.
[22] C. Arbizzani, M. Biso, D. Cericola, M. Lazzari, F. Soavi, M. Mastragostino, J. Power Sources **2008**, 185, 1575.
[23] W.-Y. Tsai, R. Lin, S. Murali, L. Zhang, J. K. McDonough, R. S. Ruoff, P.-L. Taberna, Y. Gogotsi, P. Simon, Nano Energy **2013**, 2, 403.
[24] C. Largeot, P. L. Taberna, Y. Gogotsi, P. Simon, Electrochem. Solid-State Lett. **2011**, 14, A174.
[25] L. Negre, B. Daffos, V. Turq, P. L. Taberna, P. Simon, Electrochim. Acta **2016**, 206, 490.
[26] M. H. Ryou, Y. M. Lee, J. K. Park, J. W. Choi, Adv. Mater. **2011**, 23, 3066.
[27] L. T. Zhuravlev, Colloids Surf. **2000**, 173, 1.
[28] R. A. P. O. d'Amorim, M. I. Teixeira, L. V. E. Caldas, S. O. Souza, J. Lumin. **2013**, 136, 186.
[29] J. Gelb, D. P. Finegan, D. J. L. Brett, P. R. Shearing, J. Power Sources **2017**, 357, 77.
[30] J. Zhang, Z. Liu, Q. Kong, C. Zhang, S. Pang, L. Yue, X. Wang, J. Yao, G. Cui, ACS Appl. Mater. Interfaces **2013**, 5, 128.
[31] T.-H. Cho, M. Tanaka, H. Ohnishi, Y. Kondo, M. Yoshikazu, T. Nakamura, T. Sakai, J. Power Sources **2010**, 195, 4272.
[32] W. G. Pell, B. E. Conway, J. Power Sources **2001**, 96, 57.
[33] P. L. Taberna, P. Simon, J. F. Fauvarque, J. Electrochem. Soc. **2003**, 150, A292.
[34] Y. R. Nian, H. Teng, J. Electroanal. Chem. **2003**, 540, 119.
[35] M. D. Stoller, R. S. Ruoff, Energy Environ. Sci. **2010**, 3, 1294.

Manuscript received: July 4, 2017
Revised manuscript received: August 5, 2017
Accepted manuscript online: August 21, 2017
Version of record online: ■■ ■■, 0000

B. Qin, Y. Han, Y. X. Ren, D. Sui, Y. Zhou, M. Zhang, Z. H. Sun, Y. F. Ma, Y. S. Chen*

■■ – ■■

A Ceramic-Based Separator for High-Temperature Supercapacitors

Separators for supercapacitors: Separators that can withstand temperatures higher than 350 °C and possess good tensile strength have not been reported yet. A simple and universal method for the fabrication of supercapacitor separators that can withstand over 350 °C without any shrinkage has been developed. Supercapacitors fabricated by using such a separator can be operated at 120 °C efficiently with remarkable capacitance retention.